ELSEVIER

Journal of Organometallic Chemistry 569 (1998) 109–119

Journal of Organometallic Chemistry

Reactions of the tungsten tris-sulfido complex $[PPh_4][(\eta^5\text{-}C_5Me_5)WS_3]$ with $[M'(PPh_3)_2(NO_3)]$ ($M' = Cu(I)$, $Ag(I)$), $[Au(PPh_3)Cl]$, and $[Pd(dppe)Cl_2]$: Isolation and structures of $[(\eta^5\text{-}C_5Me_5)WS_3Cu_3(PPh_3)_3(NO_3)][NO_3]$, $[\{(\eta^5\text{-}C_5Me_5)WS_3\}_2Ag_3(PPh_3)_3][NO_3]$, $[(\eta^5\text{-}C_5Me_5)WS_3Au(PPh_3)]$ and $[(\eta^5\text{-}C_5Me_5)WS_3Pd(dppe)]Cl$ (dppe = 1, 2-bis(diphenylphosphino)ethane)[1]

Jian-Ping Lang *, Hiroyuki Kawaguchi, Kazuyuki Tatsumi

Research Center for Materials Science and Department of Chemistry, Graduate School of Science, Nagoya University, Furo-cho, Chikusa-ku, Nagoya 464-8602, Japan

Received 24 March 1998

Abstract

The reactions of $[PPh_4][(\eta^5\text{-}C_5Me_5)WS_3]$ with $[M'(PPh_3)_2(NO_3)]$ ($M' = Cu(I)$ or $Ag(I)$), $[Au(PPh_3)Cl]$, and $[Pd(dppe)Cl_2]$ (dppe = 1,2-bis(diphenylphosphino)ethane) in CH_3CN yielded four new heterobimetallic clusters in good yields: $[(\eta^5\text{-}C_5Me_5)WS_3Cu_3(PPh_3)_3(NO_3)][NO_3]$ (**1**), $[\{(\eta^5\text{-}C_5Me_5)WS_3\}_2Ag_3(PPh_3)_3][NO_3]$ (**2**), $[(\eta^5\text{-}C_5Me_5)WS_3Au(PPh_3)]$ (**3**), and $[(\eta^5\text{-}C_5Me_5)WS_3Pd(dppe)]Cl$ (**4**). Analytically pure compounds **1**–**4** were characterized by spectroscopy and their crystal structures were determined by single-crystal X-ray analysis. The structure of the cation of **1** has an incomplete WS_3Cu_3 cube, and one nitrate group interacts strongly with one copper atom. The structure of the cation of **2** may be viewed as a composite of the two subcluster units, $[(\eta^5\text{-}C_5Me_5)WS_3Ag_2(PPh_3)_2]^+$ and $[(\eta^5\text{-}C_5Me_5)WS_3Ag(PPh_3)]$, which are linked by Ag–S interactions. In the structures of **3** and **4**, $Au(PPh_3)$ and Pd(dppe) fragments bridge two sulfur atoms of the common $(\eta^5\text{-}C_5Me_5)WS_3$ fragment, respectively. The behavior of **1**–**4** in solution was examined by ESI–MS.

Keywords: Sulfido complex; Tungsten; Copper; Silver; Gold; Palladium; Cluster; Crystal structures

1. Introduction

Synthesis of transition metal sulfide clusters continues to be a major objective in inorganic chemistry. Use of thiometallates is a popular method for preparation of clusters with high nuclearity, and in particular thiomolybdates and thiotungstates have served as key building blocks of various heterometallic clusters. The cluster complexes obtained from these have shown rich chemistry of their own [1–9], and they may be relevant to biological systems [10–12], industrially important catalysis [13–15], and photonic materials [16,17]. In previous studies in our laboratory, the intriguing organometallic trisulfido complex anions $[(\eta^5\text{-}C_5Me_5)MS_3]^{n-}$ ($M = Nb, Ta$ $(n = 2)$ [18,19]; $M = W, Mo$ $(n = 1)$ [20,21]) were isolated, and these trisulfido complexes were demonstrated to give rise to a series of new heterometallic cluster complexes [22–26]. For example, reactions of $[PPh_4][(\eta^5\text{-}C_5Me_5)WS_3]$ with CuX (X = NCS or Br) and AgBr produced double-

* Corresponding author. Fax: +81 52 7892943.

[1] Dedicated to Professor Akira Nakamura on the occasion of his retirement from Osaka University.

0022-328X/98/$ - see front matter
PII S0022-328X(98)00779-7

cubane clusters $[PPh_4]_2[(\eta^5\text{-}C_5Me_5)WS_3Cu_3X_3]_2$ (X = NCS or Br) and an unprecedented one-dimensional ladder polymer $[(\eta^5\text{-}C_5Me_5)WS_3Ag_2Br]_\infty$, respectively. These results prompted us to extend our understanding of cluster formation of $[(\eta^5\text{-}C_5Me_5)WS_3]^-$ with such electron-rich metals, and to compare the chemistry with that of closely related thiometallates. Thus we examined reactions of $[PPh_4][(\eta^5\text{-}C_5Me_5)WS_3]$ with $[M'(PPh_3)_2(NO_3)]$ (M′ = Cu or Ag), $[Au(PPh_3)Cl]$, and $[Pd(dppe)Cl_2]$, which resulted in four novel heterobimetallic clusters, $[(\eta^5\text{-}C_5Me_5)WS_3Cu_3(PPh_3)_3(NO_3)][NO_3]$ (**1**), $[\{(\eta^5\text{-}C_5Me_5)WS_3\}_2Ag_3(PPh_3)_3][NO_3]$ (**2**), $[(\eta^5\text{-}C_5Me_5)WS_3Au(PPh_3)]$ (**3**) and $[(\eta^5\text{-}C_5Me_5)WS_3Pd(dppe)]Cl$ (**4**). This report describes the synthesis and structures of these clusters.

2. Results and discussion

2.1. Preparations of 1–4

When three equivalents of $[Cu(PPh_3)_2(NO_3)]$ was added to a red solution of $[PPh_4][(\eta^5\text{-}C_5Me_5)WS_3]$ in CH_3CN, the color immediately darkened. The solution was allowed to stir at room temperature overnight and then concentration altered to ca. 3 ml. After layering diethyl ether onto the solution, $[(\eta^5\text{-}C_5Me_5)WS_3Cu_3(PPh_3)_3(NO_3)][NO_3]$ (**1**) was isolated as red crystals in 79% yield. Interestingly, the analogous reaction of $[PPh_4][(\eta^5\text{-}C_5Me_5)WS_3]$ with three equivalents of $[Ag(PPh_3)_2(NO_3)]$ in CH_3CN did not produce a WAg_3 tetranuclear cluster similar to **1**. Instead, an unexpected pentanuclear cluster $[\{(\eta^5\text{-}C_5Me_5)WS_3\}_2Ag_3(PPh_3)_3][NO_3]$ (**2**) was isolated in 83% yield based on $[PPh_4][(\eta^5\text{-}C_5Me_5)WS_3]$. On the other hand, the treatment of $[PPh_4][(\eta^5\text{-}C_5Me_5)WS_3]$ with one equivalent of $[Au(PPh_3)Cl]$ in CH_3CN formed a neutral binuclear cluster $[(\eta^5\text{-}C_5Me_5)WS_3Au(PPh_3)]$ (**3**). Filtration of the reaction mixture, followed by recrystallization from $CHCl_3/Et_2O$, gave **3** as orange–red prisms in 85% yield. Even if the W/Au ratio in this reaction was varied from 2 to 1/2, the 1/1 adduct **3** was the sole isolable product. In the case of the reaction between $[PPh_4][(\eta^5\text{-}C_5Me_5)WS_3]$ with $[Pd(dppe)Cl_2]$, a cationic binuclear complex $[(\eta^5\text{-}C_5Me_5)WS_3Pd(dppe)]Cl$ (**4**) was produced in 70% yield. The formation of these heterometallic sulfide clusters are summarized in Scheme 1.

Complex salts **1**, **2**, and **4** are very soluble in CH_3CN and $CHCl_3$, while **3** dissolves in toluene and $CHCl_3$. These compounds are all stable to oxygen and moisture. Since the electronic spectrum of $[PPh_4][(\eta^5\text{-}C_5Me_5)WS_3]$ in CH_3CN has a relatively strong absorption band at 377 nm, the peaks at 381 (**1**), 378 (**2**), 375 (**3**), and 374 (**4**) nm observed in the spectra of the corresponding compounds in acetonitrile or $CHCl_3$ are probably originated from sulfur–tungsten charge-transfer transitions of the common $(\eta^5\text{-}C_5Me_5)WS_3$ moiety. The ^{1}H-NMR spectra in $CDCl_3$ show a single resonance of $\eta^5\text{-}C_5Me_5$ at 1.87 (**1**), 1.91 (**2**), 2.17 (**3**), and 2.12 (**4**) ppm. The $^{31}P\{^1H\}$-NMR signals at 14.9 ppm ($w_{1/2} = 107$ Hz) for **1**, 17.8 ppm ($w_{1/2} = 315$ Hz) for **2**, and 43.6 ppm ($w_{1/2} = 39$ Hz) for **3** are somewhat broad, probably due to the couplings between the ^{31}P nuclei and the $^{63}Cu(^{65}Cu)$, $^{107}Ag(^{109}Ag)$, and ^{235}Au nuclei. In the $^{31}P\{^1H\}$-NMR spectrum of **4**, a very sharp singlet appears at 67.07 ppm. The IR spectrum of **1** displays W–S_{br} stretching vibrations at 433–409 cm^{-1}, while that of **2** shows both W–S_t stretching vibrations at 506–493 cm^{-1} and W–S_{br} stretching vibrations at

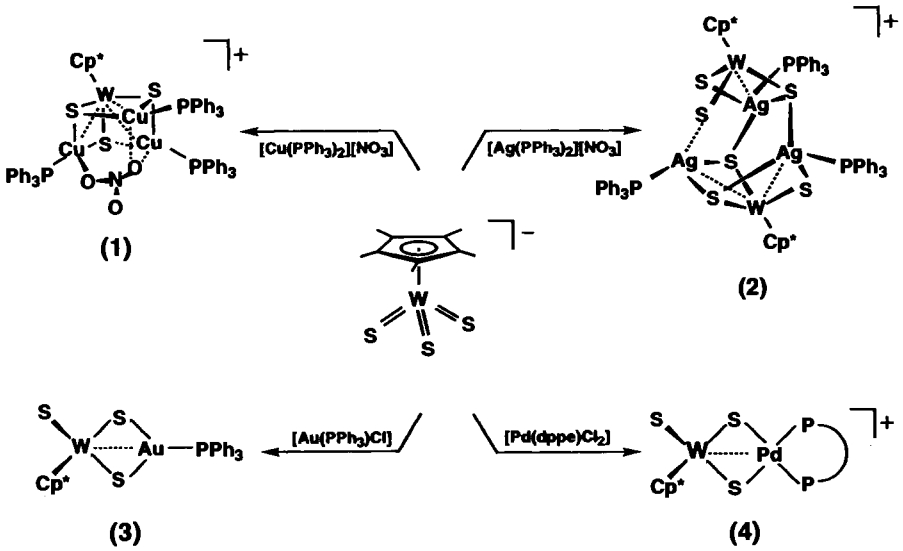

Scheme 1.

425–407 cm^{-1}. Likewise, **3** and **4** exhibit both W–S_t and W–S_{br} stretching vibrations at 506–476 (**3**) and 491 (**4**) cm^{-1}, and at 432–407 (**3**) and 419 (**4**) cm^{-1}, respectively. The IR spectra of **1** and **2** are also featured by the absorption bands arising from nitrate. As will be described later in this paper, complex **1** contains two different types of nitrates, viz., a discrete nitrate anion and a nitrate strongly bound to Cu atoms. The nitrate of **2** is a former type acting as a counter anion. The relatively broad band at 1350 cm^{-1} of **2** is unequivocally assigned to the asymmetric N–O stretching vibrational mode, which is comparable to the bands observed for $[Ag(PPh_4)_4][NO_3]$ (1340 cm^{-1}) [27] and $[NH_4][NO_3]$ (1350 cm^{-1}) [28]. In contrast, the IR spectrum of **1** shows two peaks at 1343 cm^{-1} and 1268 cm^{-1}. The former broad peak is probably originated from the discrete nitrate anion. The latter peak, which is less broad than the 1343 cm^{-1} peak, is assigned to one of the two peaks arising from the splitting of the asymmetric N–O stretching mode of the Cu-bound nitrate. Although the other peak of the splitting does not appear clearly in the spectrum, the 1436 cm^{-1} signal of the PPh_3 origin is broadened compared with the other PPh_3 bands. Therefore we assume that one Cu-bound-nitrate signal overlaps with the PPh_3 signal at 1436 cm^{-1}, to give a splitting of 168 cm^{-1} for the asymmetric N–O vibrational mode. This large splitting is consistent with strong NO_3–Cu interactions in the structure of **1**, and is comparable to the one observed for $[Cu(PPh_3)_2(NO_3]$ (200 cm^{-1}) [29,30].

2.2. Crystal structure of $[(\eta^5\text{-}C_5Me_5)WS_3Cu_3(PPh_3)_3(NO_3)][NO_3]$ (1)

According to the X-ray analysis, crystals of **1** were solvated by CH_3CN, and an asymmetric unit consists of one $[(\eta^5\text{-}C_5Me_5)WS_3Cu_3(PPh_3)_3(NO_3)]^+$ cation, one $[NO_3]^-$ anion, and one CH_3CN solvent molecule. The structure of the cation of **1** is presented in Fig. 1 with the labeling scheme, where the phenyl groups are omitted for clarity. The selected bond lengths and angles are given in Table 1. The complex cation of **1** is made of a WS_3Cu_3 incomplete cube, and a phosphine ligand is coordinated at each Cu site. The analogous WS_3Cu_3 incomplete cubane frame was reported by us in the structures of $[PPh_4]_2[(\eta^5\text{-}C_5Me_5)WS_3Cu_3X_3]_2$ (X = NCS, Br) [23]. Interestingly, one nitrate anion is strongly bound to one of the three Cu atoms, namely Cu(1). The Cu(1)–O(1) distance is as short as 2.25(2) Å, which is close to that found in $[Cu(PPh_3)_2(NO_3)]$ (2.22 Å) [30]. On the other hand, O(3) interacts weakly with Cu(2) and Cu(3), with the distances of 2.60 and 2.43 Å, respectively. The occurrence of such a triply bridging nitrate is rare. Due to the interactions with nitrate oxygen atoms, three copper atoms distort from a trigonal planar geometry by varying degrees. The

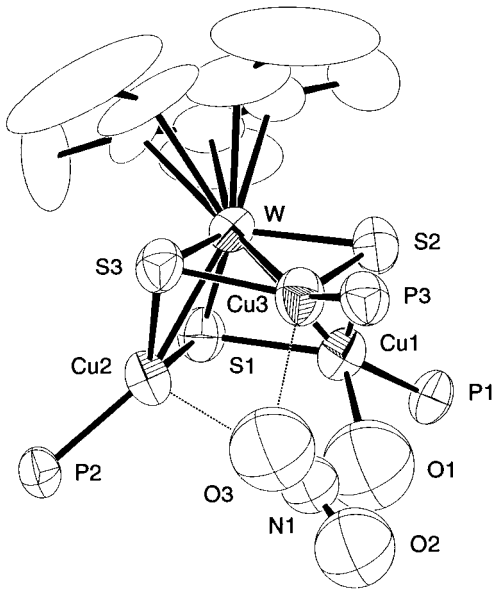

Fig. 1. Structure of the cation of **1** with the labeling scheme adopted. Thermal ellipsoids are drawn at the 50% level. Phenyl groups and hydrogen atoms are omitted for clarity.

W–Cu–P angles are 146.3(2), 157.6(2), and 160.0(2)° for Cu(1), Cu(3) and Cu(2), respectively, and the extent of the bending parallel the strength of the Cu–O interactions. The $[(\eta^5\text{-}C_5Me_5)WS_3]$ unit has a slightly distorted three-legged piano stool structure, and the S_3 plane is parallel to both the $\eta^5\text{-}C_5Me_5$ ring (dihedral angle = 179°) and the Cu_3 plane (178°). The mean W-μ_3-S bond length (2.272(4) Å) is elongated by 0.08 Å compared with that of $[PPh_4][(\eta^5\text{-}C_5Me_5)WS_3]$ [21] as a

Table 1
Selected bond lengths (Å) and angles (°) for **1**

Bond length (Å)			
W–Cu(1)	2.716(2)	W–Cu(2)	2.693(2)
W–Cu(3)	2.688(2)	W–S(1)	2.273(4)
W–S(2)	2.273(5)	W–S(3)	2.270(5)
Cu(1)–S(1)	2.256(5)	Cu(1)–S(2)	2.236(5)
Cu(2)–S(1)	2.237(5)	Cu(2)–S(3)	2.257(5)
Cu(3)–S(2)	2.253(5)	Cu(3)–S(3)	2.230(5)
Cu(1)–P(1)	2.241(5)	Cu(2)–P(2)	2.231(5)
Cu(3)–P(3)	2.218(5)	Cu(1)–O(1)	2.25(2)
Cu(2)…O(3)	2.60	Cu(3)…O(3)	2.43
N(1)–O[a]	1.18	N(2)–O*	1.15
Bond angle (°)			
S(1)–W–S(2)	105.1(2)	S(1)–W–S(3)	105.5(2)
S(2)–W–S(3)	105.5(2)	S(1)–Cu(1)–S(2)	106.9(2)
S(1)–Cu(2)–S(3)	107.1(2)	S(2)–Cu(3)–S(3)	107.5(2)
S(1)–Cu(1)–P(1)	115.2(2)	S(2)–Cu(1)–P(1)	122.0(2)
S(2)–Cu(1)–O(1)	99.3(6)	P(1)–Cu(1)–O(1)	96.0(6)
S(1)–Cu(2)–P(2)	123.5(2)	S(3)–Cu(2)–P(2)	120.7(2)
S(2)–Cu(3)–P(3)	118.1(2)	S(3)–Cu(3)–P(3)	125.0(2)
Cu(1)–O(1)–N(1)	115.(1)	W–Cu(1)–P(1)	146.3(2)
W–Cu(2)–P(2)	160.0(2)	W–Cu(3)–P(3)	157.6(2)
O–N(1)–O*	113	O–N(2)–O*	119

[a] Average value.

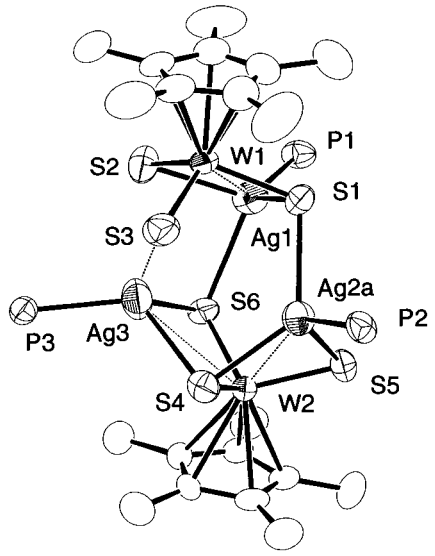

Fig. 2. Structure of the cation of **2** with 50% thermal ellipsoids. Only one of the distorted Ag(2) atom, i.e. Ag(2a), is shown, that was refined with site occupancy factor of 0.85, and phenyl groups and hydrogen atoms are omitted for clarity.

consequence of the co-ordination to Cu atoms. The W–Cu distances of 2.688(3)–2.716(2) Å are comparable to those of $[PPh_4]_2[(\eta^5\text{-}C_5Me_5)WS_3Cu_3Br_3]_2$ (2.649(1)–2.6762(8) Å) [23] and $[WOS_3Cu_2(PPh_3)_3]\cdot 0.8CH_2Cl_2$ (2.659(3)–2.816(3) Å) [31], suggesting the presence of a dative interaction between the W(VI) and Cu(I) centers. The mean Cu–S distance (2.245(5) Å) is comparable to those found in $[PPh_4]_2[(\eta^5\text{-}C_5Me_5)WS_3Cu_3Br_3]_2$ (2.234(2) Å) [23] and $[WOS_3Cu_2(PPh_3)_3]\cdot 0.8CH_2Cl_2$ (2.295(6) Å) [31]. The Cu–P lengths (2.218(5)–2.241(5) Å) are normal.

2.3. Crystal structure of $[\{(\eta^5\text{-}C_5Me_5)WS_3\}_2Ag_3(PPh_3)_3][NO_3]$ (2)

Crystals of **2** are again solvated by CH_3CN. The nitrate group acts as counter anion, and does not interact with the complex cation. The refinement of the structure showed that Ag(2) was disordered over two positions, Ag(2a) and Ag(2b), and their occupancy factors were refined to 0.85/0.15. The core structure with the minor Ag(2b) position is practically the same as that with Ag(2a), and the low occupancy of Ag(2b) did not allow us to find the minor PPh_3 position connected to Ag(2b). Fig. 2 shows the view of major configuration of the cation with Ag(2a) and the minor structure with Ag(2b) is provided in Supplement Materials. The selected bond lengths and angles of the major configuration are given in Table 2. In the figure, the phenyl groups of phosphine ligands are omitted for clarity. The structure of the complex cation may be regarded as a composite of the two subcluster units, $[(\eta^5\text{-}C_5Me_5)WS_3Ag_2(PPh_3)_2]^+$ and $[(\eta^5\text{-}C_5Me_5)WS_3Ag(PPh_3)]$, and they are connected in a complicated way through Ag–S interactions. These inter-unit Ag–S lengths vary from Ag(2a)–S(1) = 2.663(3) Å to Ag(3)–S(3) = 2.89 Å, while the Ag–S lengths within each unit range from 2.503(3) to 2.664(3) Å. Due to the varying degrees of Ag–S interactions, the W–S bond distances are also diverse, where W(1)–S(3) and W(2)–S(5) bonds are substantially shorter than the others. The W–Ag distances are long, ranging from 3.016(1) to 3.18 Å, which are longer than those found in the related structures of $[\alpha\text{-MePyH}]_\infty[WS_4Ag]_\infty$ (2.948(1) Å) [32] and $[WS_4Ag_2(PPh_3)_3]\cdot 0.8CH_2Cl_2$ (2.971(2) Å) [33]. Therefore, the dative bonds between the $d^{10}W^{VI}$ and d^0Ag^I centers in **2** are weak, if any. All the Ag–P lengths fall in the normal range.

The reactions between $[(\eta^5\text{-}C_5Me_5)WS_3]^-$ with $[M'(PPh_3)_2(NO_3)]$ (M′ = Cu, Ag) turned out to produce very different types of clusters. Oxophilicity of Cu(I) appears to be higher than that of Ag(I), and the fourth co-ordination site of the Cu atoms in **1** tends to be occupied by a nitrate oxygenation. On the other hand, the Ag center(s) of either $[(\eta^5\text{-}C_5Me_5)WS_3Ag(PPh_3)]$ or $[(\eta^5\text{-}C_5Me_5)WS_3Ag_2(PPh_3)_2]$ fragment in **2**, favor interactions with S atoms of the other fragment. The inter-fragment Ag–S interactions bind the two fragments

Table 2
Selected bond lengths (Å) and angles (°) for **2**

Bond length (Å)			
W(1)…Ag(1)	3.023(1)	W(2)…Ag(2a)	3.016(1)
W(2)…Ag(3)	3.18	W(1)–S(1)	2.260(2)
W(1)–S(2)	2.245(3)	W(1)–S(3)	2.181(2)
W(2)–S(4)	2.267(2)	W(2)–S(5)	2.186(2)
W(2)–S(6)	2.242(2)	Ag(1)–S(1)	2.503(3)
Ag(1)–S(2)	2.569(3)	Ag(1)–S(6)	2.715(2)
Ag(2a)–S(1)	2.663(3)	Ag(2a)–S(4)	2.530(3)
Ag(2a)–S(5)	2.565(3)	Ag(3)–S(4)	2.590(3)
Ag(3)–S(6)	2.664(3)	Ag(3)…S(3)	2.89
Ag(1)–P(1)	2.417(2)	Ag(2a)–P(2)	2.412(3)
Ag(3)–P(3)	2.445(2)	N–O*	1.20
Bond angle (°)			
S(1)–W(1)–S(2)	109.99(9)	S(1)–W(1)–S(3)	105.58(9)
S(2)–W(1)–S(3)	103.8(1)	S(4)–W(2)–S(5)	107.13(9)
S(4)–W(2)–S(6)	108.99(9)	S(5)–W(2)–S(6)	104.52(9)
S(1)–Ag(1)–S(2)	93.37(8)	S(1)–Ag(1)–S(6)	109.38(7)
S(1)–Ag(1)–P(1)	124.17(9)	S(2)–Ag(1)–S(6)	89.92(8)
S(1)–Ag(2a)–S(4)	123.37(8)	S(1)–Ag(2a)–S(5)	99.41(8)
S(1)–Ag(2a)–P(2)	106.65(9)	S(4)–Ag(2a)–S(5)	89.36(8)
S(4)–Ag(3)–S(6)	88.63(8)	S(4)–Ag(3)–P(3)	118.33(8)
S(6)–Ag(3)–P(3)	120.63(9)	W(1)–S(1)–Ag(2a)	106.62(9)
Ag(1)–S(1)–Ag(2a)	104.20(9)	Ag(2a)–S(4)–Ag(3)	93.01(8)
W(2)–S(6)–Ag(1)	114.9(1)	Ag(1)–S(6)–Ag(3)	86.37(8)
O(2)–N(1)–O(3)*	112		

[a] Average value.

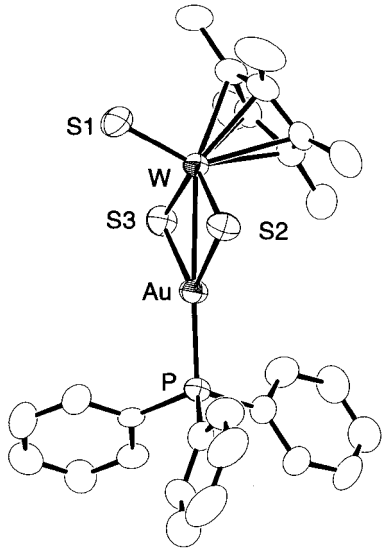

Fig. 3. Molecular structure of **3** with 50% thermal ellipsoids. Hydrogen atoms are omitted for clarity.

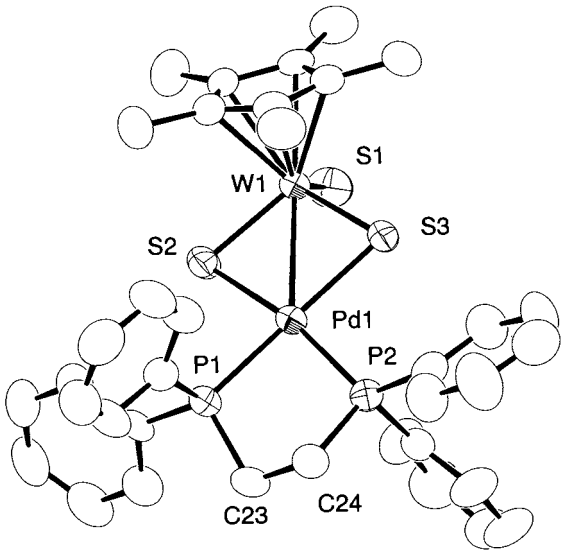

Fig. 4. Structure of the cation of **4** with 50% thermal ellipsoids. Hydrogen atoms are omitted for clarity.

tightly, and they are not dissociated easily even in solution according to the ESI–MS analysis as will be described later.

2.4. Crystal structure of $[(\eta^5\text{-}C_5Me_5)WS_3Au(PPh_3)]$ (3)

The molecular structure of **3** is shown in Fig. 3, and the important bond lengths and angles are given in Table 3. The $[Au(PPh_3)]^+$ unit bridges two S atoms of $[(\eta^5\text{-}C_5Me_5)WS_3]^-$, and the whole structure of **3** resembles a cluster subunit of **2**, $[(\eta^5\text{-}C_5Me_5)WS_3Ag(PPh_3)]$. The co-ordination geometry at gold is exactly trigonal planar, and the sum of the angles about Au is 360°. The acute angles at S(2) and S(3), Au–S(2)–W 74.82(7)° and Au–S(3)–W 74.40(8)°, and the relatively short Au–W distance of 2.8279(5) Å, suggest a gold-to-tungsten dative interaction. The observed Au–W distance is close to those of $[WS_4(AuCH_2PPh_3)_2]$ (2.820(2) Å) [34] and $[WS_4(AuPPh_2CH_3)_2]$ (2.840(1) Å) [35]. The mean Au–S length (2.394(3) Å) and the Au–P length (2.440(3) Å) are normal.

Table 3
Selected bond lengths (Å) and angles (°) for **3**

Bond length (Å)			
Au–W	2.8279(5)	W–S(1)	2.151(3)
W–S(2)	2.274(3)	W–S(3)	2.264(3)
Au–S(2)	2.379(3)	Au–S(3)	2.409(3)
Au–P	2.263(2)		
Bond angle (°)			
S(1)–W–S(2)	104.8(1)	S(1)–W–S(3)	103.3(1)
S(2)–W–S(3)	109.37(9)	W–Au–P	172.20(6)
S(2)–Au–S(3)	101.29(9)	S(2)–Au–P	134.48(9)
S(3)–Au–P	124.04(9)	Au–S(2)–W	74.82(7)
Au–S(3)–W	74.40(8)		

2.5. Crystal structure of $[(\eta^5\text{-}C_5Me_5)WS_3Pd(dppe)]Cl$ (4)

The X-ray analysis of **4** showed that an asymmetric unit consists of two crystallographically independent $[(\eta^5\text{-}C_5Me_5)WS_3Pd(dppe)]^+$ cations, two Cl^- anions, and two CH_3CN solvent molecules. Each of the two discrete Cl^- anions are disordered with the occupancy factors of 0.7/0.3. Because the two cluster cations are structurally very similar, only one of them is presented in Fig. 4. The pertinent bond distances and angles of the two structures are compared in Table 4. The main fragment of $[(\eta^5\text{-}C_5Me_5)WS_3Pd(dppe)]^+$ is similar to that of the related neutral complex $[WS_4Pd(dppe)]$ [36], where a $[Pd(dppe)]^{2+}$ fragment bridges two sulfur atoms of $[(\eta^5\text{-}C_5Me_5)WS_3]^-$. The palladium atom adopts a square-planar coordination geometry with two P atoms of dppe and two S atoms of $[(\eta^5\text{-}C_5Me_5)WS_3]^-$. The average W–S–Pd angle (78.3_) is 2.3° larger than that in $[\{(allyl)Pd\}_2WS_4]$ (allyl = η^3-C_3H_5) (76.0°) [37], and the mean W–Pd length of 2.9042(8) Å is 0.1 Å longer. Therefore, the interaction between W(VI) and Pd(II) in **4** is somewhat weaker. The average Pd–S bond length of 2.342(2) Å is comparable to those of $[WS_4Pd(dppe)]$ (2.353(5) Å) and $[\{(allyl)Pd\}_2WS_4]$ (2.340(6) Å), and the mean Pd–P distance (2.290(3) Å) is normal.

2.6. Comparison of $[MO_nS_{4-n}]^{2-}$ (M = Mo, W; n = 0, 1) and $[(\eta^5\text{-}C_5Me_5)WS_3]^-$ in the reactions with phosphine complexes of the coinage-metal cations M′ (M′ = Cu, Ag, Au)

It is interesting to compare the W/M′/S (M′ = Cu(I), Ag(I), Au(I)) clusters reported in this paper with

those obtained from the reactions between thiometallates and phosphine (or arsine) complexes of the coinage metals. The sulfide clusters derived from $[MS_4]^{2-}$ or $[MOS_3]^{2-}$ (M = Mo, W) can be classified into the following three types: (1) $[MM'_2S_3EL_n]$ (E = S, O; M′ = Cu(I), Ag(I), Au(I); L = phosphine or arsine; $n = 2, 3, 4$) (linear or bent MM'_2 structures) [1,6–9,34,38–42]; (2) $[MM'_3S_3EL_3X]$ (M′ = Cu(I), Ag(I); X = Cl, Br, I) (cubane core structures) [1,6–9,38]; $[(MS_3E)_2M'_4L_4]$ (M′ = Cu(I), Ag(I)) (face-shared double-cubane core structures) [8,43–46]. The general structural features deduced from the above clusters are the followings. Firstly, that nearly all of these clusters are neutral. Secondly, that the core structures of M/Cu clusters and M/Ag clusters are very much alike. Thirdly, that the nuclearity of M/Au(I)/S clusters seldom exceed four. On the other hand, the cluster forming reactions of $[(\eta^5\text{-}C_5Me_5)WS_3]^-$ resulted in the cationic tetranuclear WCu_3 cluster **1**, the cationic pentanuclear W_2Ag_3 cluster **2**, and the neutral dinuclear WAu complex **3**, respectively. The structure of **1** is to some extent similar to the cubane core structure of $[MM'_3S_3EL_3X]$, while **2** finds no analogue in the related thiometallate chemistry. Although a 1:1 W/Au adduct is unprecedented among thiometallate systems, the structure of **3** is close to that of $[MSe_4Au(PPhMe_2)]^-$ (M = Mo, W) [47].

2.7. Electrospray ionization mass spectra of *1–4*

The ESI mass spectroscopy is known to provide a convenient method for characterization of metal clusters in solution [26,48–54]. We examined the ESI mass spectra of **1–4** in order to gain insight into their behavior in solution. The measurements of ESI mass spectra for complex salts, **1**, **2**, and **4** in CH_3CN were straightforward. Their positive-ion spectra show unequivocally the parent cluster cations and the fragment species. Table 5 lists the observed peak with relative intensities, where only the highest peak in each isotopic cluster is given. The assignments were made by inspection of peak positions and isotopic distributions.

Table 4
Selected bond lengths (Å) and angles (°) for **4**

Bond length (Å)			
W(1)–Pd(1)	2.9127(9)	W(2)–Pd(2)	2.8956(8)
W(1)–S(1)	2.151(3)	W(2)–S(4)	2.140(3)
W(1)–S(2)	2.255(2)	W(2)–S(5)	2.253(3)
W(1)–S(3)	2.252(3)	W(2)–S(6)	2.252(2)
Pd(1)–S(2)	2.334(3)	Pd(2)–S(5)	2.344(2)
Pd(1)–S(3)	2.352(3)	Pd(2)–S(6)	2.340(3)
Pd(1)–P(1)	2.292(3)	Pd(2)–P(3)	2.281(3)
Pd(1)–P(2)	2.299(3)	Pd(2)–P(4)	2.286(2)
Bond angle (°)			
S(1)–W(1)–S(2)	105.5(1)	S(4)–W(2)–S(5)	105.9(1)
S(1)–W(1)–S(3)	105.3(1)	S(4)–W(2)–S(6)	104.5(1)
S(2)–W(1)–S(3)	104.08(9)	S(5)–W(2)–S(6)	104.44(9)
S(2)–Pd(1)–S(3)	98.64(9)	S(5)–Pd(2)–S(6)	98.94(9)
S(2)–Pd(1)–P(1)	86.35(9)	S(5)–Pd(2)–P(3)	89.00(9)
S(3)–Pd(1)–P(2)	91.02(9)	S(6)–Pd(2)–P(4)	86.79(9)
P(1)–Pd(1)–P(2)	84.55(9)	P(3)–Pd(2)–P(4)	85.23(9)
W(1)–S(2)–Pd(1)	78.78(8)	W(2)–S(5)–Pd(2)	78.06(8)
W(1)–S(3)–Pd(1)	78.48(8)	W(2)–S(6)–Pd(2)	78.15(8)

The positive ion ESI mass spectrum of **1** shows a set of ion peaks associated with the parent molecular ion $[(\eta^5\text{-}C_5Me_5)WS_3Cu_3(PPh_3)_3(NO_3)]^+$, and the observed isotopic cluster matches very well with the theoretical isotopic abundance as shown in Fig. 5. In addition to this parent ion signal, there appeared four sets of peaks assignable to $[(\eta^5\text{-}C_5Me_5)WS_3Cu_3(PPh_3)_2(NO_3)]^+$, $[(\eta^5\text{-}C_5Me_5)WS_3Cu_2(PPh_3)_2]^+$, $[(\eta^5\text{-}C_5Me_5)WS_3Cu_2(PPh_3)]^+$, and $[Cu(PPh_3)_2]^+$. The former four fragment cations are formed by a loss of one or two phosphine, one copper atom, and/or nitrate, under the mass condition. We did not detect a dicationic species, $[(\eta^5\text{-}C_5Me_5)WS_3Cu_3(PPh_3)_3]^{2+}$, which would be formed upon removal of a nitrate anion. Therefore the nitrate anion seems to be bound strongly to the copper atom(s), and its elimination takes place with a concomitant loss of one copper atom and one phosphine.

In the case of the positive ion ESI mass spectrum of **2**, the parent ion signal for $[\{(\eta^5\text{-}C_5Me_5)WS_3\}_2Ag_3(PPh_3)_3]^+$, which is presented in Fig. 6 along with the calculated isotopic pattern, accompanying the signals arising from a series of fragment ions. The fragmentation occurs with a consecutive liberation of phosphine ligands. Apparently the silver atoms are tightly bound to the $(\eta^5\text{-}C_5Me_5)WS_3$ fragments. The absence of fragment cations of the type $[\{(\eta^5\text{-}C_5Me_5)WS_3\}_2Ag_n(PPh_3)_n]^+$ suggests that the W_2Ag_3 core structure remains intact under the mass condition. One the other hand, the mass spectrum of **4** exhibits only the parent cation signal, and the chelate phosphine ligand resists being liberated.

Measurements of mass spectra for neutral complexes are not usually easy, and that was the case for **3**. However, addition of equimolar amount of LiCl to a THF solution of **3** allowed us to obtain positive ion signals which were assigned to $[(\eta^5\text{-}C_5Me_5)WS_3Au(PPh_3)Li]^+$ and $[(\eta^5\text{-}C_5Me_5)WS_3Au(PPh_3)Li(THF)]^+$. The cationic species, Li^+ and $Li(THF)^+$, are probably bound to the bridging sulfur atom(s). Again, no fragmentation of the parent complex of **3** occurred.

3. Concluding remarks

Four new W/M′ (M′ = Cu, Ag, Au, Pd) clusters **1–4** were prepared in high yields by the use of the tri-sulfido complex anion $[(\eta^5\text{-}C_5Me_5)WS_3]^-$ as a building component. Their crystal structures were established by X-ray

Table 5
Electrospray ionization mass spectral data for **1–4**[a]

Compound		Peak (m/z)[b]	Relative intensity (%)
1	$[(\eta^5\text{-}C_5Me_5)WS_3Cu_3(PPh_3)_3(NO_3)]^+$	1454.2	16
	$[(\eta^5\text{-}C_5Me_5)WS_3Cu_3(PPh_3)_2(NO_3)]^+$	1192.0	39
	$[(\eta^5\text{-}C_5Me_5)WS_3Cu_2(PPh_3)_2]^+$	1067.2	100
	$[(\eta^5\text{-}C_5Me_5)WS_3Cu_2(PPh_3)]^+$	805.0	14
	$[Cu(PPh_3)_2]^+$	587.2	83
2	$[\{(\eta^5\text{-}C_5Me_5)WS_3\}_2Ag_3(PPh_3)_3]^+$	1941.1	4
	$[\{(\eta^5\text{-}C_5Me_5)WS_3\}_2Ag_3(PPh_3)_2]^+$	1679.1	100
	$[\{(\eta^5\text{-}C_5Me_5)WS_3\}_2Ag_3(PPh_3)]^+$	1417.0	47
	$[\{(\eta^5\text{-}C_5Me_5)WS_3\}_2Ag_3]^+$	1155.0	9
	$[Ag(PPh_3)_2]^+$	631.1	2
3	$[(\eta^5\text{-}C_5Me_5)WS_3Au(PPh_3)Li]^+$	881.2	100
	$[(\eta^5\text{-}C_5Me_5)WS_3Au(PPh_3)Li(THF)]^+$	953.2	17.5
4	$[(\eta^5\text{-}C_5Me_5)WS_3Pd(dppe)]^+$	920.9	100

[a] ESI mass spectra were recorded at cone voltage of 20 V for **1–3**, and 25 V for **4**. The concentration of the samples in CH_3CN is ca. 0.4 M for **1**, and ca. 0.3 M for **2** and **4**. In the case of **3**, the concentration for either **3** or the LiCl additive in THF is ca. 0.3 M.
[b] Only the highest peak in each isotope cluster is presented.

crystallography, and the ESI mass spectra were measured in order to investigate their behavior in solution. The successful isolation of W/M′/S clusters **1–4**, coupled with our related study [23–26], shows that $[(\eta^5\text{-}C_5Me_5)WS_3]^-$ serves as a versatile starting reagent for the synthesis of various heterometallic sulfide clusters, which are different from those derived from thiotungstate. Further investigation of this aspect is currently underway in our laboratory.

4. Experimental section

4.1. General procedure

All manipulations were carried out under argon using standard Schlenk-line techniques. $[M'(PPh_3)_2(NO_3)]$ (M′ = Cu(I) [29], Ag(I) [27]) and $[Pd(dppe)Cl_2]$ [55] were prepared according to the literature methods. $[Au(PPh_3)Cl]$ was purchased from Aldrich Chemicals and used without further purification. All solvents were pre-dried over activated molecular sieves and refluxed over the appropriate drying agents under argon. The elemental analyses for C, H, N and S were performed on a LECO-CHNS microanalyzer. FTIR spectra in the range 4000–400 cm^{-1} were recorded on a Perkin Elmer 2000 FTIR spectrophotometer using KBr pellets. ^1H and $^{31}P\{^1H\}$-NMR spectra were recorded at an ambient temperature on a Varian UNITYplus-500 spectrometer. ^1H-NMR chemical shifts were referenced to the $CDCl_3$ or CD_2Cl_2 signal, and $^{31}P\{^1H\}$-NMR chemical shifts were relative to 85% H_3PO_4. UV-vis spectra were measured on JASCO V-560 spectrophotometer. Electrospray ionization (ESI) mass spectra were recorded on an API 300 Triple Quadruple LC/MS/MS mass spectrometer (Perkin–Elmer Sciex Instruments). Samples were introduced to the spectrometer as a CH_3CN (**1**, **2**, **4**) or a THF (**3**) solution (ca. 0.3–0.4 M) at a flow rate of 3 μl min^{-1} using a syringe pump (Harvard Apparatus). The electrospray probe capillary was maintained at a potential of 3.5 kV and the orifice to the skimmer potential (cone voltage) was varied from 20 to 25 V.

4.2. Synthesis of $[(\eta^5\text{-}C_5Me_5)WS_3Cu_3(PPh_3)_3(NO_3)][NO_3]$ (1)

$[Cu(PPh_3)_2(NO_3)]$ (0.20 g, 0.3 mmol) was added to a solution of $[PPh_4][(\eta^5\text{-}C_5Me_5)WS_3]$ (0.076 g, 0.10 mmol) in 20 ml of CH_3CN. The red solution immediately darkened, which was allowed to stir overnight at room temperature. The resulting homogeneous solution was concentrated to ca. 3 ml in vacuo and diethyl ether (6 ml) was added. Red prisms of $\mathbf{1}\cdot CH_3CN$ were formed in two days, and they were collected by filtration, washed with CH_3CN/Et_2O (1:5), and then dried in vacuo. Yield: 0.12 g (79.1%). Anal. calc. for $C_{64}H_{60}Cu_3N_2O_6P_3S_3W$: C, 50.68; H, 4.00; N, 1.85; S, 6.34. Found: C, 50.97; H, 4.03; N, 2.14; S, 6.56%. ^1H-NMR ($CDCl_3$, 500 MHz): δ 7.26–7.52 (m, 45H, Ph), 1.87 (s, 15H, $\eta^5\text{-}C_5Me_5$). $^{31}P\{^1H\}$-NMR ($CDCl_3$): δ 14.9 ($w_{1/2} = 107$ Hz). IR (KBr disc, cm^{-1}): 1481 (s), 1436 (s, br), 1384 (s), 1343 (s, br), 1268 (s, br), 1097 (s), 1026 (m), 997 (m), 830 (w), 744 (s), 693 (s), 523 (s), 432 (m), 409 (m). UV-vis (CH_3CN) (λ_{max}/nm (ε/$M^{-1}cm^{-1}$)): 381 (5800).

4.3. Synthesis of $[\{(\eta^5\text{-}C_5Me_5)WS_3\}_2Ag_3(PPh_3)_3][NO_3]$ (2)

$[Ag(PPh_3)_2(NO_3)]$ (0.28 g, 0.39 mmol) was added to a solution of $[PPh_4][(\eta^5\text{-}C_5Me_5)WS_3]$ (0.10 g, 0.13 mmol) in 20 ml of CH_3CN. The red solution immediately turned dark. From a workup similar to that used for isolation of **1**, dark red prisms of $\mathbf{2}\cdot CH_3CN$ were formed after three days, which were collected by filtration, washed with CH_3CN/Et_2O (1: 5), and dried in vacuo. Yield: 0.11 g (82.8%). Anal. calc. for $C_{74}H_{75}Ag_3NO_3P_3S_6W_2$: C, 44.37; H, 3.78; N, 0.69; S, 9.60. Found: C, 44.58; H, 3.81; N, 1.09; S, 9.86%. ^{1}H-NMR ($CDCl_3$, 500 MHz): δ 7.36–7.49 (m, 45H, Ph), 1.91 (s, 30H, η^5-C_5Me_5). $^{31}P\{^1H\}$-NMR ($CDCl_3$): δ 17.8 ($w_{1/2} = 315$ Hz). IR (KBr disc, cm^{-1}): 1479 (s), 1435 (s), 1384 (s), 1350 (s, br), 1096 (s), 1026 (m), 996 (m), 847 (w), 756 (s), 742 (s), 693 (s), 516 (s), 506 (m), 493 (w), 425 (m), 407 (s). UV-vis (CH_3CN) (λ_{max}/nm (ε/$M^{-1}cm^{-1}$)): 378 (17400).

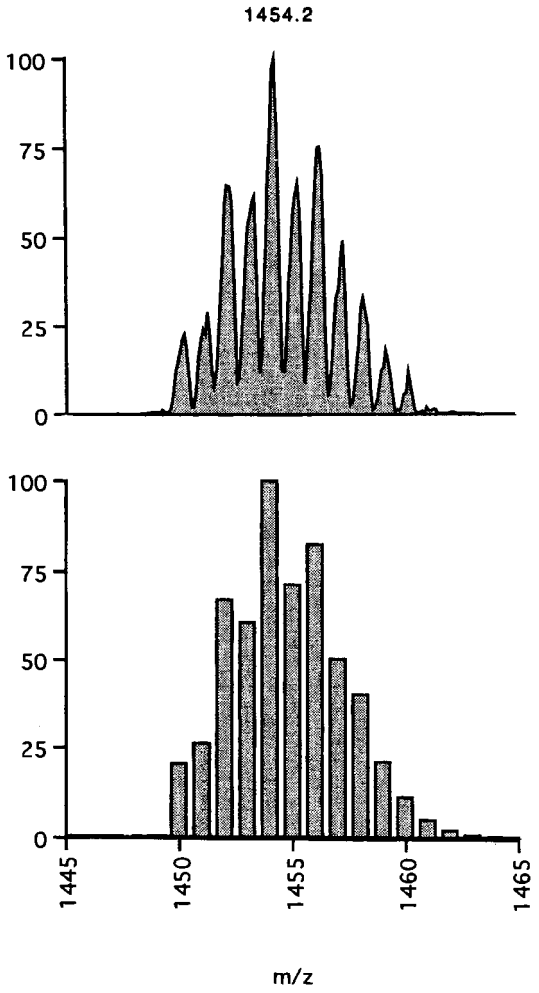

Fig. 5. The positive-ion ESI mass spectrum (top) and the calculated isotope pattern (below) of $[(\eta^5\text{-}C_5Me_5)WS_3Cu_3(PPh_3)_3(NO_3)]^+$.

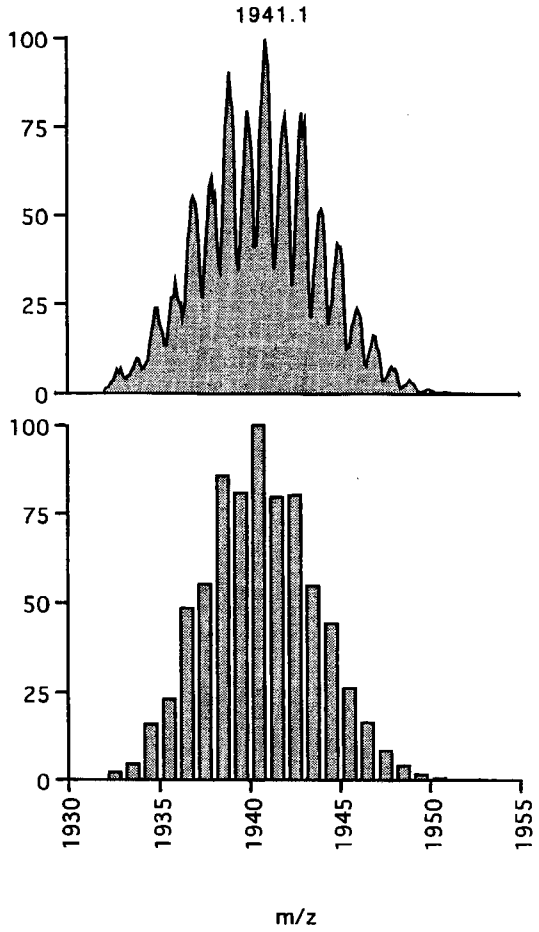

Fig. 6. The positive-ion ESI mass spectrum (top) and the calculated isotope pattern (below) of $[\{(\eta^5\text{-}C_5Me_5)WS_3\}_2Ag_3(PPh_3)_3]^+$.

4.4. Synthesis of $[(\eta^5\text{-}C_5Me_5)WS_3Au(PPh_3)]$ (3)

A CH_3CN solution (15 ml) of $[Au(PPh_3)Cl]$ (0.07 g, 0.15 mmol) was added to a solution of $[PPh_4][(\eta^5\text{-}C_5Me_5)WS_3]$ (0.11 g, 0.15 mmol) in CH_3CN (15 ml), and an orange–red solid was immediately precipitated. The mixture was stirred for 3 h at room temperature and then filtered. Recrystallization of the resulting orange–red solid from $CHCl_3/Et_2O$ produced orange–red prisms of $\mathbf{3}\cdot CHCl_3$, which were collected by filtration, washed with $CHCl_3/Et_2O$ (1:4), and dried in vacuo. Yield: 0.12 g (84.6%). Anal. calc. for $C_{28}H_{30}AuPS_3W$: C, 38.45; H, 3.46; S, 11.00. Found: C, 38.49, H, 3.42; S, 11.27. ^{1}H-NMR (CD_2Cl_2, 500 MHz): δ 7.48–7.72 (m, 15H, Ph), 2.17 (s, 15H, η^5-C_5Me_5). $^{31}P\{^1H\}$-NMR ($CDCl_3$): δ 43.6 ($w_{1/2} = 39$ Hz). IR (KBr disc, cm^{-1}): 1479 (s), 1434 (s), 1374(s), 1180 (m), 1094 (s), 1025 (m), 997 (m), 906(w), 753 (s), 740 (s), 693 (s), 531 (s), 506 (s), 476 (s), 432 (w), 407 (m). UV-vis ($CHCl_3$) (λ_{max}/nm (ε/$M^{-1}cm^{-1}$)): 375 (9700).

4.5. Synthesis of $[(\eta^5\text{-}C_5Me_5)WS_3Pd(dppe)]Cl$ (4)

A red CH_3CN solution (15 ml) of $[PPh_4][(\eta^5\text{-}C_5Me_5)$-

Table 6
Crystallographic data for $1\cdot CH_3CN$, $2\cdot CH_3CN$, $3\cdot CHCl_3$, and $4\cdot CH_3CN$

	$1\cdot CH_3CN$	$2\cdot CH_3CN$	$3\cdot CHCl_3$	$4\cdot CH_3CN$
Formula	$C_{66}H_{63}Cu_3N_3O_6P_3S_3W$	$C_{76}H_{78}Ag_3N_2O_3P_3S_6W_2$	$C_{29}H_{31}AuCl_3PS_3W$	$C_{38}H_{42}ClNP_2PdS_3W$
M	1557.83	2044.05	993.89	996.58
Crystal system	Monoclinic	Triclinic	Orthorhombic	Triclinic
Space group	$P2_1/c$	$P\bar{1}$	$Pbca$	$P\bar{1}$
a (Å)	12.701(2)	16.770(8)	14.453(4)	14.005(2)
b (Å)	13.442(3)	17.629(7)	22.968(9)	31.938(4)
c (Å)	40.036(6)	14.850(4)	19.748(4)	9.311(2)
α (°)		106.98(3)		98.07(1)
β (°)	91.51(1)	108.38(3)		93.47(2)
γ (°)		96.98(3)		99.15(1)
V (Å^3)	6833(2)	3872(2)	6555(2)	4056(1)
Z	4	2	8	2
λ(Mo–K$_\alpha$) (Å)	0.71069	0.71069	0.71069	0.71069
D_{calc} (g·cm^{-3})	1.51	1.75	2.01	1.63
μ (cm^{-1})	28.1	39.8	85.0	36.1
$2\theta_{max}$ (°)	50.0	50.0	55.0	45.0
Total reflections	11967	12214	7841	11371
Number of observations ($I>3.00\sigma(I)$)	4560	8306	3533	8783
Number of variables	711	865	343	815
$\Delta\rho_{max}/\Delta\rho_{min}$ (e Å^{-3})	0.85/−0.62	1.62/−1.46	0.57/−1.20	1.94/−1.32
R^a	0.057	0.036	0.032	0.043
R_w^b	0.064	0.050	0.036	0.055
GOF^c	1.71	2.41	1.29	2.05

[a] $R = \Sigma||F_o|-|F_c||/\Sigma|F_o|$.
[b] $R_w = \{\Sigma w(|F_o|-|F_c|)^2/\Sigma w|F_o|^2\}^{1/2}$.
[c] GOF $= \{\Sigma w(|F_o|-|F_c|)^2/(n-p)\}^{1/2}$, where n is the number of reflections and p is the total number of parameters refined.

WS_3] (0.11g, 0.15 mmol) was added to a slurry of [Pd(dppe)Cl_2] (0.16 g, 0.30 mmol) in CH_3CN (15 ml). The solution became orange–red immediately, and the mixture was allowed to stir overnight at room temperature. Removal of unreacted [Pd(dppe)Cl_2] by filtration, followed by a standard workup gave orange–red plates of $4\cdot CH_3CN$, which were collected by filtration, washed with CH_3CN/Et_2O (1:5), and dried in vacuo. Yield: 0.10 g (69.8%). Anal. calc. for $C_{36}H_{39}ClP_2PdS_3W$: C, 45.25; H, 4.12; S, 10.07. Found: C, 45.48, H, 4.32; S, 9.76. ^{1}H-NMR ($CDCl_3$, 500 MHz): δ 7.48–7.66 (m, 20H, Ph), 3.15–3.40 (m, 4H, PCH_2CH_2P), 2.12 (s, 15H, η^5-C_5Me_5). $^{31}P\{^1H\}$-NMR ($CDCl_3$): δ 67.1. IR (KBr disc, cm^{-1}): 1482 (m), 1434 (m), 1377 (m), 1185 (m), 1103 9s), 1025 (m), 997 (m), 878 (m), 820 (m), 750 (s), 719 (s), 707 (s), 690 (s), 532 (s), 491 (s), 419 (m). UV-vis (CH_3CN) (λ_{max}/nm (ε/M^{-1} cm^{-1})): 419 (2700), 374 (7600), 305 (17000).

4.6. Crystal structure determinations of *1*, *2*, *3*, and *4*

X-ray quality crystals of $1\cdot CH_3CN$, $2\cdot CH_3CN$, $3\cdot CHCl_3$, and $4\cdot CH_3CN$ were obtained from the preparations as described above. Diffraction data were collected on a Rigaku AFC7R diffractometer at room temperature using graphite-monochromatized Mo–K$_\alpha$ radiation (0.71079 Å). A red prism of $1\cdot CH_3CN$ with dimensions $0.25\times0.15\times0.20$ mm, an orange–red prism of $3\cdot CHCl_3$ with dimensions $0.70\times0.30\times0.35$ mm, and an orange–red plate of $4\cdot CH_3CN$ with dimensions $0.80\times0.20\times0.15$ mm were sealed in capillaries under argon, respectively, while a dark red prism of $2\cdot CH_3CN$ with dimensions $0.50\times0.35\times0.40$ mm was put on a glass fiber. Cell constants and an orientation matrix for data collection were obtained from least-squares refinements using the setting angles of 25 carefully centered reflections (22 reflections in the case of $2\cdot CH_3CN$) in the range $6.4°<2\theta<24.8°$ for $1\cdot CH_3CN$, $22.6°<2\theta<24.5°$ for $2\cdot CH_3CN$, $6.3°<2\theta<23.9°$ for $3\cdot CHCl_3$, and $8.2°<2\theta<24.8°$ for $4\cdot CH_3CN$. In all cases, the intensities of three reflections monitored every 150 reflections showed no sign of significant decay. A total of 11967 ($1\cdot CH_3CN$), 12214 ($2\cdot CH_3CN$), 7841 ($3\cdot CHCl_3$) and 11371 ($4\cdot CH_3CN$) reflections were collected. An empirical absorption correction using the ψ scan technique was applied, which resulted in transmission factors ranging from 0.62 to 1.00 for $1^{\bullet}CH_3CN$, from 0.44 to 1.00 for $2\cdot CH_3CN$, from 0.41 to 1.00 for $3\cdot CHCl_3$, and from 0.56 to 1.00 for $4\cdot CH_3CN$. The data were also corrected for Lorentz and polarization effects.

The structure of $1\cdot CH_3CN$ was solved by heavy-atom Patterson methods [56], while the structures of $2\cdot CH_3CN$, $3\cdot CHCl_3$ and $4\cdot CH_3CN$ were solved by

direct methods [57,58] and expanded using Fourier techniques [59]. All non-hydrogen atoms were refined anisotropically except for $[NO_3]^-$ and CH_3CN in $\mathbf{1}\cdot CH_3CN$, and two CH_3CN molecules and two disordered Cl atoms in $\mathbf{4}\cdot CH_3CN$. All hydrogen atoms were put at calculated positions without refinement. For $\mathbf{1}\cdot CH_3CN$, the comparatively high thermal parameters for the C atoms of η^5-C_5Me_5 group may be due to disorder. However attempts to model the disorder failed. N, O, and C atoms in two $[NO_3]^-$ anions and a CH_3CN molecule were refined isotropically with high thermal parameters. Neutral atom scattering factors were taken from Cromer and Waber [60]. Anomalous dispersion effects were included in F_c [61]. Crystallographic calculations were carried out with a teXsan crystallographic software package of the Molecular Structure Corp. (1985 and 1992). Crystallographic data for $\mathbf{1}\cdot CH_3CN$, $\mathbf{2}\cdot CH_3CN$, $\mathbf{3}\cdot CHCl_3$, and $\mathbf{4}\cdot CH_3CN$ are summarized in Table 6. Listings of atomic co-ordinates and thermal parameters for compounds **1**–**4** are given as supplement materials.

5. Supplement materials available

Tables of crystal and refinement data, atomic co-ordinates, thermal parameters, bond lengths and angles, least-squares planes, structure drawing with atom numbering schemes, unit cell and packing diagrams (59 pages) of **1**–**4** are available from the authors on request.

Acknowledgements

J.-P. Lang would like to thank the Japan Society for the Promotion of Science (JSPS) for a post-doctoral fellowship.

References

[1] A. Müller, E. Diemann, R. Jostes, H. Bögge, Angew. Chem. Int. Ed. Engl. 20 (1981) 934.
[2] R.H. Holm, Pure Appl. Chem. 67 (1995) 2117.
[3] D. Coucouvanis, Acc. Chem. Res. 24 (1991) 1.
[4] E.I. Stiefel, D. Coucouvanis, W.E. Newton, Molybdenum Enzymes, Cofactors and Model Systems; ACS Symp. Ser. 535, Am. Chem. Soc., Washington, DC, (1993).
[5] K.E. Howard, T.B. Rauchfuss, A.L. Rheingold, J. Am. Chem. Soc. 108 (1986) 297.
[6] G. Christou, C.D. Garner, F.E. Mabbs, T.J. King, J. Chem. Soc., Chem. Commun. 740 (1978).
[7] Y. Jeannin, F. Sécheresse, S. Bernes, F. Robert, Inorg. Chim. Acta 198-200 (1992) 493.8.
[8] H.-W. Hou, X.-Q. Xin, S. Shi, Coord. Chem. Rev. 153 (1996) 25.
[9] J.-P. Lang, X.-Q. Xin, J. Solid State Chem. 108 (1994) 118.
[10] R.H. Holm, Chem. Soc. Rev. 10 (1981) 455.
[11] E.I. Stiefel, K. Matsumoto, Transition Metal Sulfur Chemistry, Biological and Industrial Significance, ACS Symp. Ser. 653, Am. Chem. Soc., Washington, DC, (1996).
[12] C.F. Mills, Philos. Trans. R. Soc. Lond. Ser. B 288 (1979) 51.
[13] R.R. Chianelli, T.A. Picoraro, T.R. Halbert, W.H. Pan, E.I. Stiefel, J. Catal. 86 (1984) 226.
[14] T.B. Rauchfuss, Prog. Inorg. Chem. 39 (1991) 259.
[15] M.D. Curtis, Appl. Organomet. Chem. 6 (1992) 429.
[16] S. Shi, W. Ji, S.-H. Tang, J.-P. Lang, X.-Q. Xin, J. Am. Chem. Soc. 116 (1994) 3615.
[17] J.-P. Lang, K. Tatsumi, H. Kawaguchi, J.-M. Lu, P. Ge, W. Ji, S. Shi, Inorg. Chem. 35 (1996) 7924.
[18] K. Tatsumi, Y. Inoue, A. Nakamura, R.E. Cramer, W. VanDoorne, J.W. Gilje, J. Am. Chem. Soc. 111 (1989) 782.
[19] K. Tatsumi, Y. Inoue, H. Kawaguchi, M. Kohsaka, A. Nakamura, R.E. Cramer, W. VanDoorne, G.J. Taogoshi, P.N. Richmann, Organometallics 12 (1993) 352.
[20] H. Kawaguchi, K. Tatsumi, J. Am. Chem. Soc. 117 (1995) 3885.
[21] H. Kawaguchi, K. Yamada, J.-P. Lang, K. Tatsumi, J. Am. Chem. Soc. 119 (1997) 10346.
[22] K. Tatsumi, H. Kawaguchi, Y. Inoue, A. Nakamura, R.E. Cramer, J.A. Golen, Angew. Chem. Int. Ed. Engl. 32 (1993) 32.
[23] J.-P. Lang, H. Kawaguchi, S. Ohnishi, K. Tatsumi, J. Chem. Soc., Chem. Commun. 405 (1997).
[24] J.-P. Lang, H. Kawaguchi, K. Tatsumi, Inorg. Chem. 36 (1997) 6447.
[25] J.-P. Lang, K. Tatsumi, Inorg. Chem. 37 (1998) 160.
[26] J.-P. Lang, H. Kawaguchi, S. Ohnishi, K. Tatsumi, Inorg. Chim. Acta 1998, (in press).
[27] P.F. Barron, J.C. Dyason, P.C. Healy, L.M. Engelharelt, B.W. Skelton, A.H. White, J. Chem. Soc. Dalton Trans. 1965 (1986).
[28] K. Nakamoto, Infrared Spectra of Inorganic and Coordination Compounds, Wiley, New York, 1963, p. 92.
[29] F.A. Cotton, D.M.L. Goodgame, J. Chem. Soc. 5267 (1960).
[30] G.G. Messmer, G.J. Palenik, Inorg. Chem. 8 (1969) 2570.
[31] A. Müller, U. Schimanski, J. Schimanski, Inorg. Chim. Acta 76 (1983) 245.
[32] J.-P. Lang, J.-G. Li, S.-A. Bao, X.-Q. Xin, Polyhedron 12 (1993) 801.
[33] A. Müller, H. Bögge, E.Z. Koniger-Ahlborn, Naturforschung B 34 (1979) 1698.
[34] F. Canales, M.C. Gimeno, P.G. Jones, A. Laguna, J. Chem. Soc., Dalton Trans. 439 (1997).
[35] J.C. Huffmann, R.S. Roth, A.R. Siedle, J. Am. Chem. Soc. 98 (1976) 4340.
[36] B. Wu, W.-J. Zheng, X.-Y. Huang, X.-T. Wu, S.-Y. Yu, Polyhedron 16 (1997) 801.
[37] K.E. Howard, T.B. Rauchfuss, S.R. Wilson, Inorg. Chem. 27 (1988) 3561.
[38] A. Müller, H. Bögge, U. Schimanski, Inorg. Chim. Acta 69 (1983) 5.
[39] J.K. Stallick, A. Siedle, A.D. Mighell, C. Hubbard, J. Am. Chem. Soc. 101 (1979) 2903.
[40] A. Müller, R. Menge, Z. Anorg. Allg. Chem. 393 (1972) 259.
[41] E.M. Kinsch, D.W. Stephan, Inorg. Chim. Acta 96 (1985) 87.
[42] J.M. Charnock, S. Bristow, J.R. Nicholson, L.D. Garner, W. Clegg, J. Chem. Soc., Dalton Trans. 303 (1987).
[43] A. Müller, H. Bögge, E. Koniger-Ahlborn, W. Hellmann, Inorg. Chem. 18 (1979) 2301.
[44] A. Müller, H. Bögge, E. Koniger-Ahlborn, J. Chem. Soc., Chem. Commun. 739 (1987).
[45] A. Müller, H. Bögge, T. Hwang, Inorg. Chim. Acta 39 (1980) 73.
[46] R. Doherty, C.R. Hubbard, A.D. Mighell, A.R. Siedle, J. Stewart, Inorg. Chem. 18 (1979) 2991.

[47] R.J. Salm, A. Misetic, J.A. Ibers, Inorg. Chim. Acta 240 (1995) 239.
[48] J.B. Fenn, M. Mann, C.K. Meng, S.F. Wong, C.M. Whitehouse, Science 246 (1989) 64.
[49] R.D. Smith, J.A. Loo, C.G. Edmonds, C.J. Barinaga, H.R. Udseth, Anal. Chem. 62 (1990) 882.
[50] I.G. Dance, K.J. Fisher, Prog. Inorg. Chem. 41 (1994) 637.
[51] T. Lover, W. Henderson, G.A. Bowmaker, J.M. Seakins, R.P. Cooney, Inorg. Chem. 36 (1997) 3711.
[52] J.-S. Huang, S. Mukerjee, B.M. Segal, H. Akashi, J. Zhou, R.H. Holm, J. Am. Chem. Soc. 119 (1997) 8662.
[53] H.R. Heveda, R.H. Holm, Inorg. Chem. 36 (1997) 4571.
[54] H. Kawaguchi, K. Yamada, S. Ohnishi, K. Tatsumi, J. Am. Chem. Soc. 119 (1997) 10871.
[55] W.L. Steffen, G.J. Palenik, Inorg. Chem. 15 (1976) 2432.
[56] P.T. Beurskens, G. Admiraal, G. Beurskens, W.P. Bosman, S. Garcia-Granda, R.O. Gould, J.M.M. Smits, C. Smykalla, PATTY: The DIRDIF program system, Technical Report of the Crystallography Laboratory, University of Nijmegen, The Netherlands, (1992).
[57] G.M. Shedrick, SHELXS86, In: G.M. Shedrick, C. Kruger, R. Goddard, (Eds), Crystallography Computing 3, Oxford University Press, Oxford, UK, (1986).
[58] A. Altomare, M.C. Burla, M. Camalli, M. Cascarano, C. Giacovazzo, A. Guagliardi, G. Polidori, SIR92. J. Appl. Cryst. 27 (1994) 435.
[59] P.T. Beurskens, G. Admiraal, G. Beurskens, W.P. Bosman, R. de Gelder, R. Israel, J.M.M. Smits, DIRDIF94: The DIRDIF-94 program system, Technical Report of the Crystallography Laboratory, University of Nijmegen, The Netherlands, (1992).
[60] D.T. Cromer, J.T. Waber, International Tables for X-ray Crystallography, Kynoch Press, Birmingham, (1974) Vol. 4.
[61] J.A. Ibers, W.C. Hamilton, Acta Crystallogr. 17 (1964) 781.